Behnaz Lahijani, Kambiz Hedayati* and Mojtaba Goodarzi

Magnetic $PbFe_{12}O_{19}$-TiO_2 nanocomposites and their photocatalytic performance in the removal of toxic pollutants

https://doi.org/10.1515/mgmc-2017-0055
Received November 14, 2017; accepted June 21, 2018; previously published online July 28, 2018

Abstract: In this work, the $PbFe_{12}O_{19}$ nanoparticles were prepared by the simple and optimized precipitation method with different organic surfactants and capping agents. In the next step, the TiO_2 nanoparticles were synthesized using the sol-gel method. At the final step, the $PbFe_{12}O_{19}$-TiO_2 nanocomposites were prepared via the sol-gel method. The effect of the precipitating agent on the morphology and particle size of the products was investigated. The prepared products were characterized by X-ray diffraction, scanning electron microscopy, transmission electron microscopy and Fourier transform infrared spectroscopy. The results obtained by the vibrating sample magnetometer show the magnetic properties of the ferrite nanostructures. The photocatalytic effect of the $PbFe_{12}O_{19}$-TiO_2 nanocomposite on the elimination of the azo dyes (acid black, acid violet and acid blue) under ultraviolet light irradiation was evaluated. The results indicate that the prepared nanocomposites have acceptable magnetic and photocatalytic performance.

Keywords: magnetic; nanocomposite; nanostructures; $PbFe_{12}O_{19}/TiO_2$; photocatalyst.

Introduction

In recent years, nanomaterials have gained research attention because of their interesting properties and applications (Gawande et al., 2014; Jafari et al., 2014). Magnetic materials have been studied extensively due to their potential use in catalytic, biomedical and environmental remediation (Moumen and Pileni, 1996; Song and Zhang, 2004; Xiao et al., 2007). Ferrite materials are a group of magnetic materials that can be divided into three classes: ferrite spinel, ferrite garnet and hexagonal ferrite (Masoumi et al., 2016). Polycrystalline hexagonal ferrites and their derivatives have attracted considerable attention in recent years. They demonstrate very high uniaxial magnetic anisotropy, making them an ideal permanent magnetic material, which can compete technically with metallic permanent magnets for some applications (Ebrahimi et al., 2017). The M-type hexa ferrites are denoted as $PbFe_{12}O_{19}$ and are widely studied because of their properties, such as large magneto crystalline anisotropy, high saturation magnetization and coercivity, recording media, permanent magnets and components in microwave and high frequency devices; hence, they have garnered research attention due to their potential applications in various fields (Thompson and Evans, 1993; Yang et al., 2007; Chaudhury et al., 2008). However, the growth of the industry worldwide has tremendously increased the generation and accumulation of waste products. This has caused environmental problems that, in turn, have become a major concern for the public.

Meanwhile, photocatalysis has gained substantial attention due to its potential environmental applications towards water treatment, such as the purification of polluted air and wastewater streams, production of self-cleaning materials and the creation of new chemicals (Fujishima and Honda, 1972; Hoffmann et al., 1995; Peral et al., 1997). The visible light photocatalysis of wastewater has also become a popular research topic due to its flexibility and cost-effective breakdown of harmful organic molecules at ambient conditions. During the photocatalytic process, when the photons with sufficient energy collide and are absorbed on the catalyst, this leads to the excitation of electrons from the valence band to the conduction band, thus producing electron-hole pairs. The photo-generated holes will form hydroxyl radicals when they react with the OH^-/water over the surface of the catalyst. These active radicals induce the degradation of the organic compounds in the air and water streams (Matthews, 1990; Linsebigler et al., 1995). Semiconductor materials, which use ultra violet (UV) irradiation to decompose organic pollutants and toxic dyes into non-toxic products by photodegradation technique, have attracted considerable attention in the last few years (Hedayati et al., 2016). The

***Corresponding author: Kambiz Hedayati,** Department of Science, Arak University of Technology, Arak 381351177, Iran, e-mail: K-hedayati@arakut.ac.ir
Behnaz Lahijani and Mojtaba Goodarzi: Department of Science, Arak University of Technology, Arak 381351177, Iran

photocatalytic properties of a semiconductor depend on the position of the energetic levels, the lifetime of the photogenerated electrons and holes, the light absorption coefficient and the nature of the interface (Augugliaro et al., 2010). The TiO_2 is a semiconductor that, in the past two decades, has been used in a variety of fields like sensors, including the production of sensitive solar cells and so on (Clark and Sutin, 1977; Hamnett et al., 1979; Cosnier et al., 1997). TiO_2 has three crystalline phases, namely, anatase, rutile and brookite, among which the rutile is the most thermodynamically stable (Li et al., 2004). These three crystalline phases have the same fundamental structural octahedral units with different arrangements (Liu et al., 2005). The anatase and brookite phases are semi-stable and converted to the rutile phase when heated (Zhang et al., 2000). The band gap of the TiO_2 is commonly a range of 3.0–3.2 eV and the wavelength is about 400 nm. This means that UV light radiation with a wavelength of less than 400 nm can stimulate the electrons and initiate a photo-reaction (Mutzhas et al., 1981).

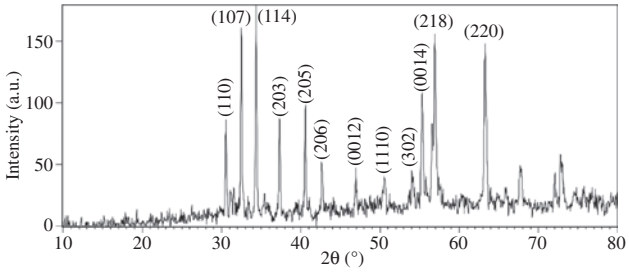

Figure 1: The XRD pattern of the $PbFe_{12}O_{19}$ nanoparticles.

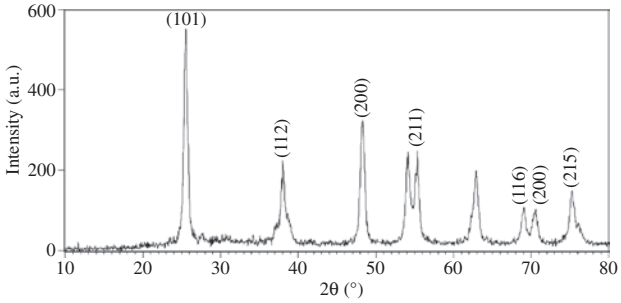

Figure 2: The XRD pattern of the TiO_2 nanoparticles.

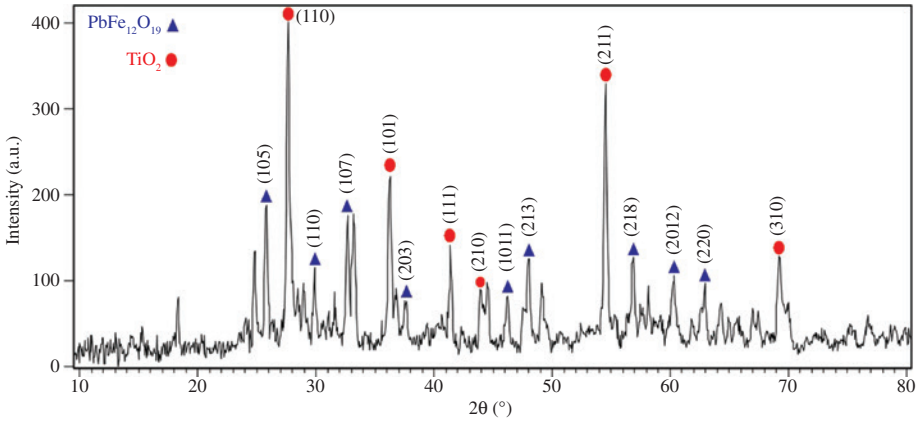

Figure 3: The XRD pattern of the $PbFe_{12}O_{19}$-TiO_2 nanocomposites.

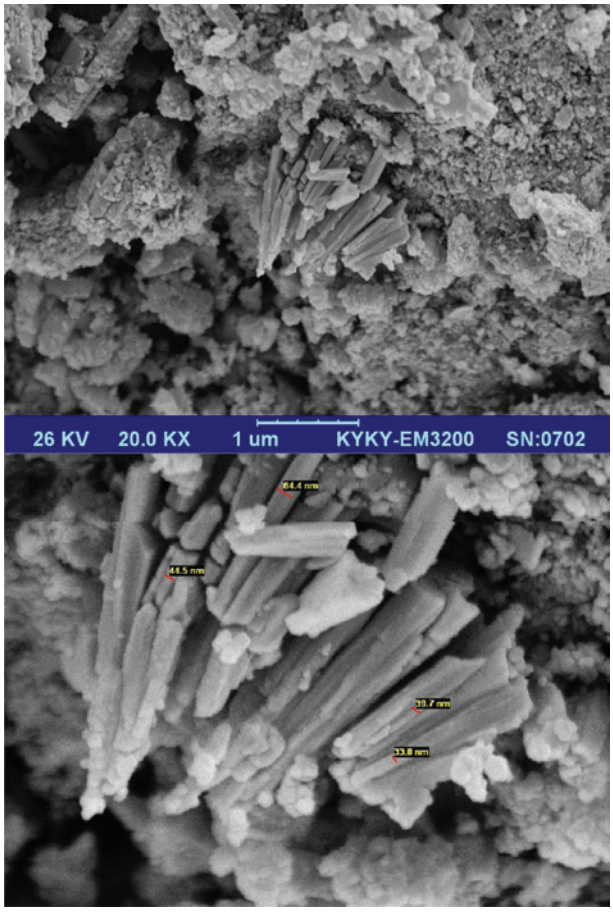

Figure 4: The SEM images of the $PbFe_{12}O_{19}$ nanoparticles prepared without any surfactant.

There are several methods that can be used to carry out the synthesis and growth of TiO_2 structures with controllable demands. The sol-gel method is one of the best candidates for TiO_2 synthesis because it provides high purity, homogeneity and low-temperature processing (Liu et al., 2012; Xin et al., 2014; Ghanbari et al., 2016).

The present study describes a synthesis and characterization of the $PbFe_{12}O_{19}$ ferrite nanoparticles using the precipitation method. Then, the TiO_2 nanoparticles and $PbFe_{12}O_{19}$-TiO_2 nanocomposite was synthesized with the sol-gel method. Finally, the photocatalytic properties and degradation of the azo dyes in the presence of this magnetic nanocomposite under UV irradiation were investigated.

Results and discussion

The structure and composition of the $PbFe_{12}O_{19}$ nanoparticles were investigated. The results are shown in Figure 1. As can be seen, the XRD pattern of the $PbFe_{12}O_{19}$ reveals the typical diffraction pattern of pure hexagonal phase (JCPDS No.: 15-0623) with the P63-mmc space group. In Figure 2, the pattern of the TiO_2 nanoparticles is indexed as a pure tetragonal phase (JCPDS No.: 04-0477) with I41-amd space group. From this, the crystallite phase of the TiO_2 nanoparticle was determined. The composition of the $PbFe_{12}O_{19}$-TiO_2 nanocomposite was also discussed. The formation of two hexagonal phase (JCPDS No.: 15-0623) and pure tetragonal phase (JCPDS No.: 04-0477) is confirmed and shown in Figure 3. As can be seen, the size of the crystals was calculated using the X-ray diffraction (XRD) data obtained from the Debye-Sherrer equation given by

$$D = \frac{0.9\,\lambda}{\beta\cos\theta},$$

where D is the size of the crystal, β is the width of the observed diffraction peak at its half maximum intensity (FWHM) and θ is the angle relation in degrees. Upon calculation, a crystalline size of 88 nm was obtained.

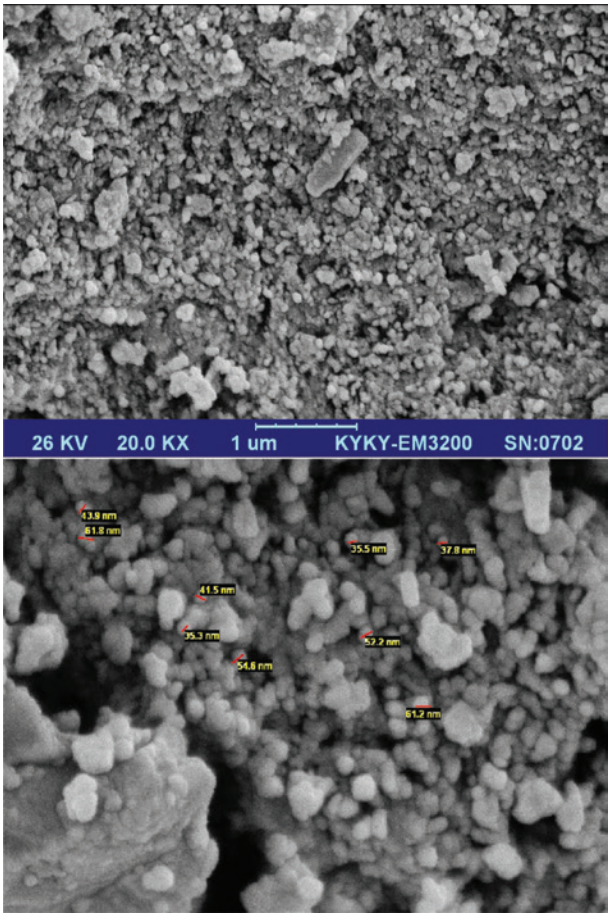

Figure 5: The SEM images of the $PbFe_{12}O_{19}$ nanoparticles synthesized with salicylic acid.

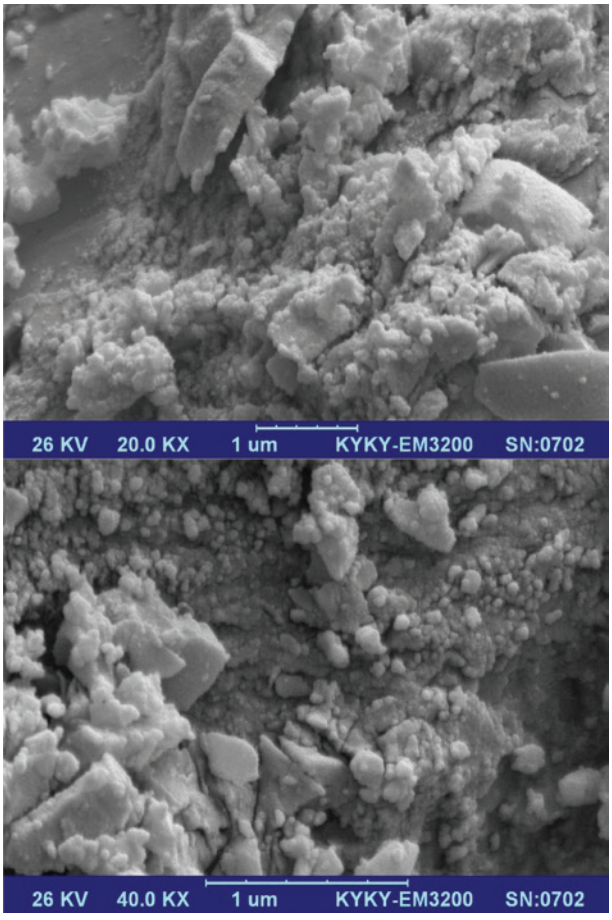

Figure 6: The SEM images of the $PbFe_{12}O_{19}$ nanoparticles synthesized with glucose.

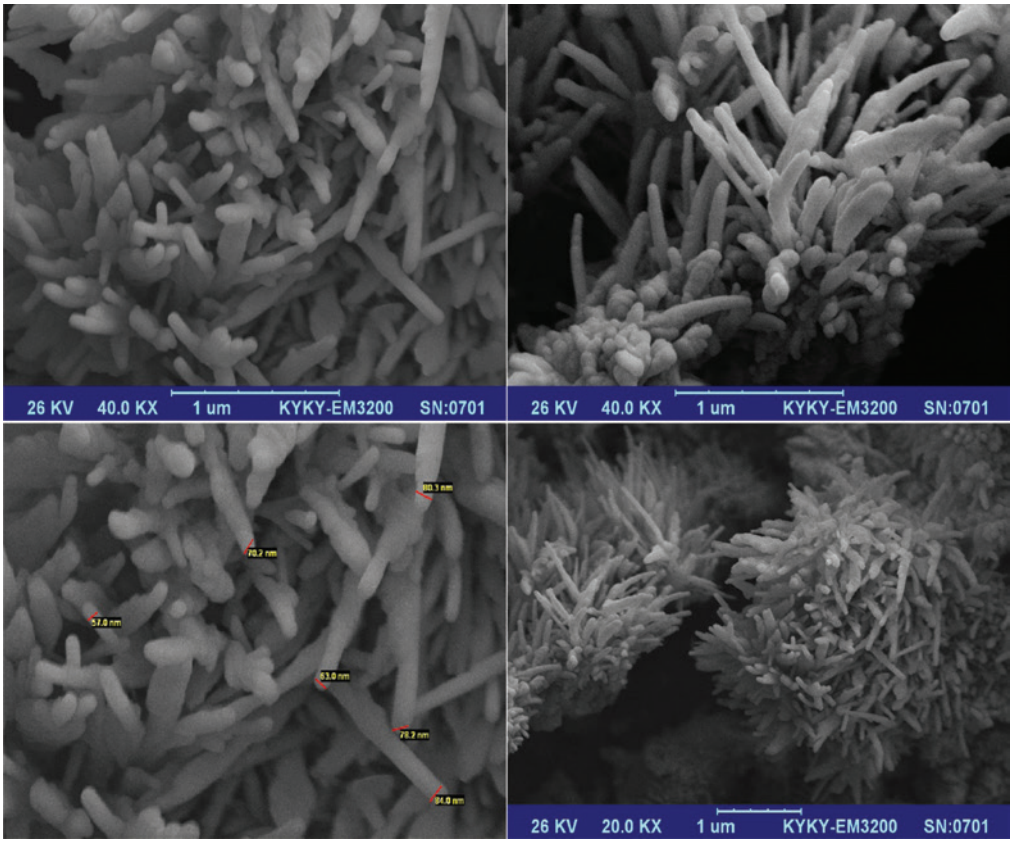

Figure 7: The SEM images of the $PbFe_{12}O_{19}$ nanoparticles synthesized in the presence of gelatin.

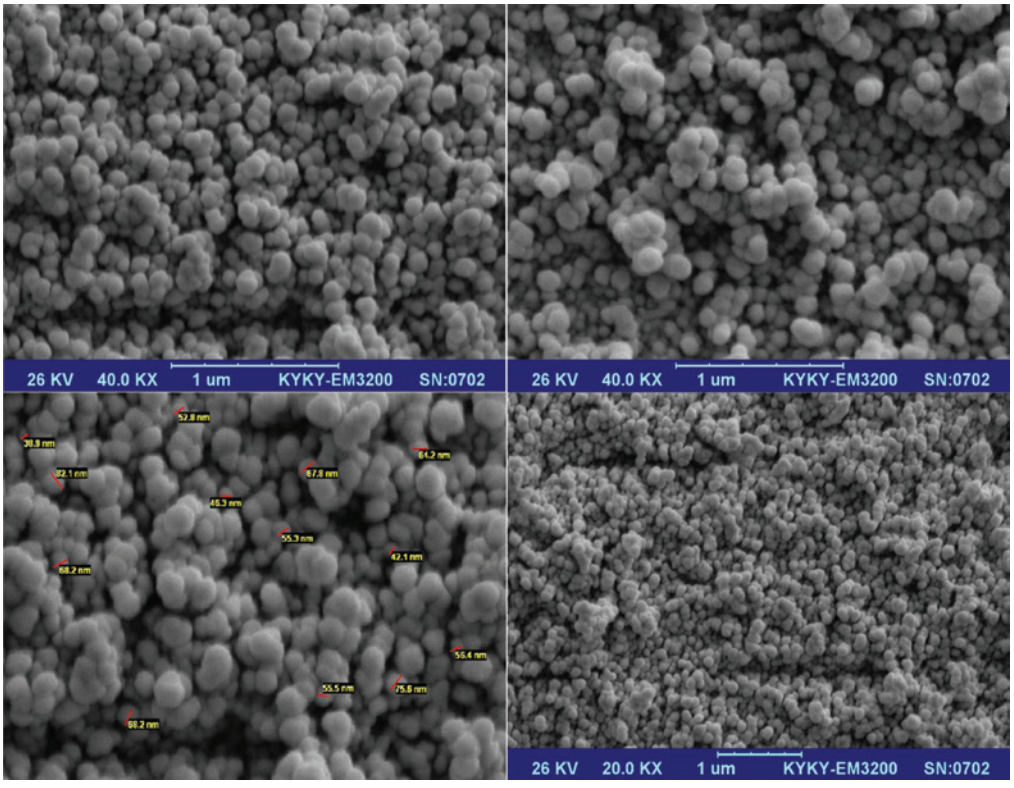

Figure 8: The SEM images of the $PbFe_{12}O_{19}$ nanoparticles synthesized in the presence of starch.

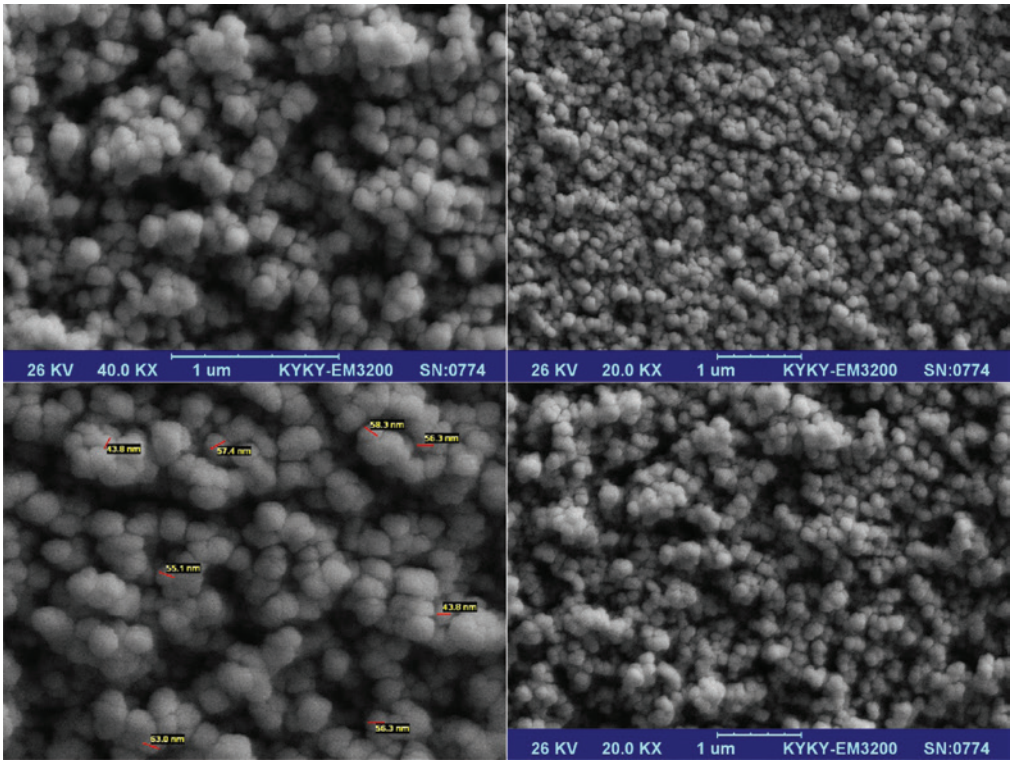

Figure 9: The SEM images of the TiO_2 nanoparticles via the sol-gel method.

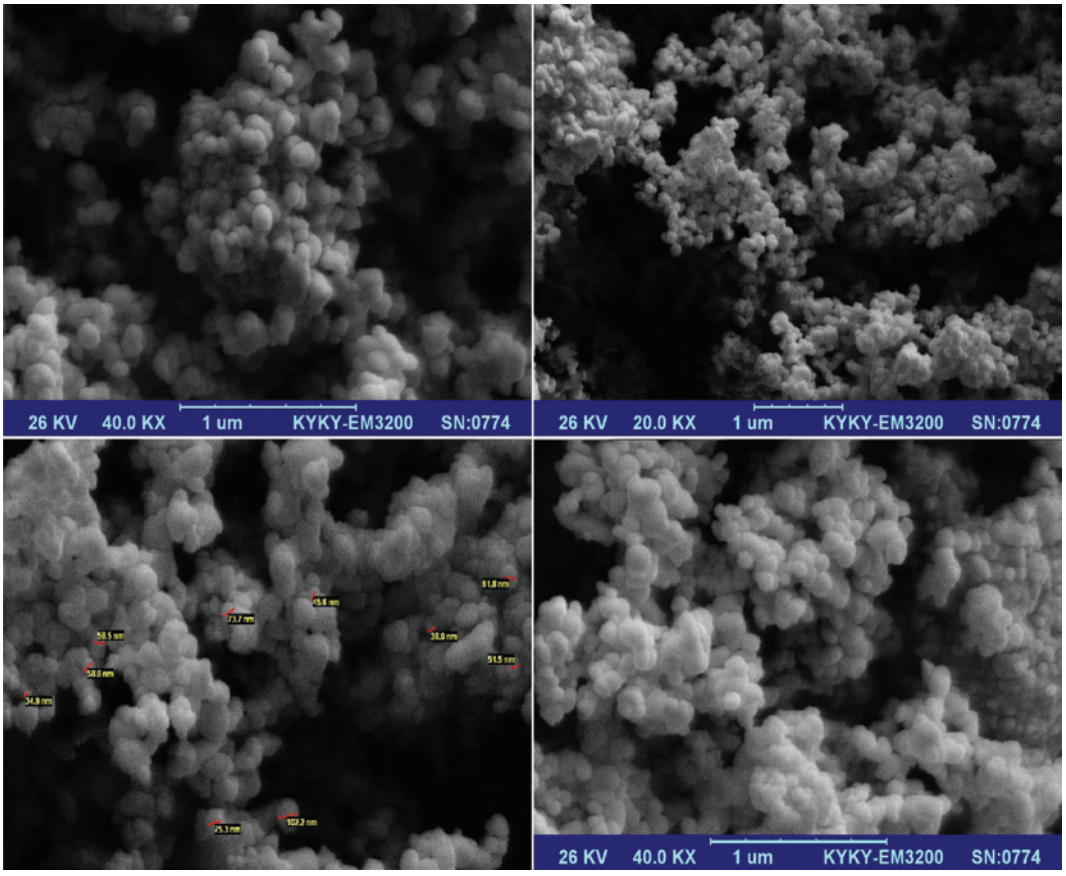

Figure 10: The SEM images of the $PbFe_{12}O_{19}$-TiO_2 nanocomposites.

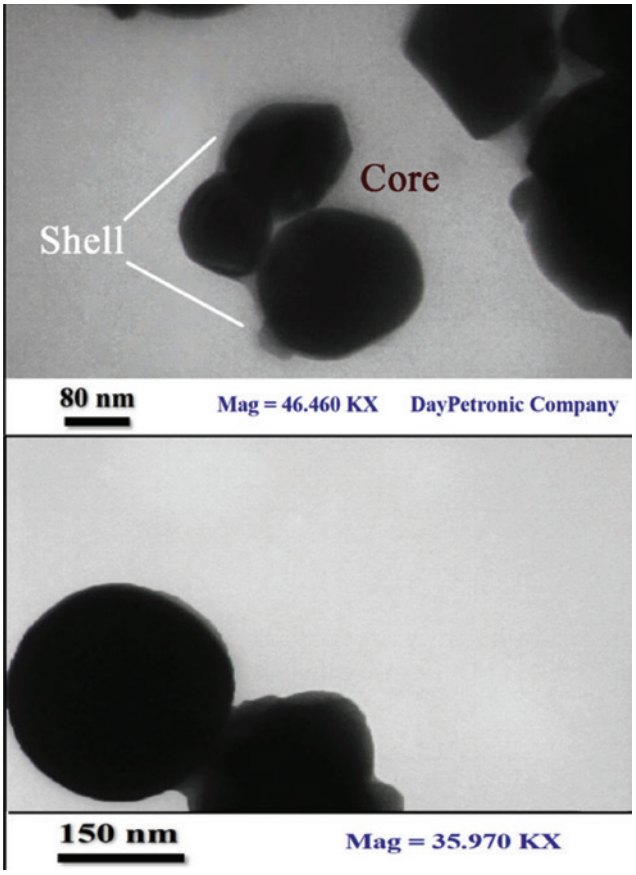

Figure 11: The TEM images of the $PbFe_{12}O_{19}/TiO_2$ nanocomposites.

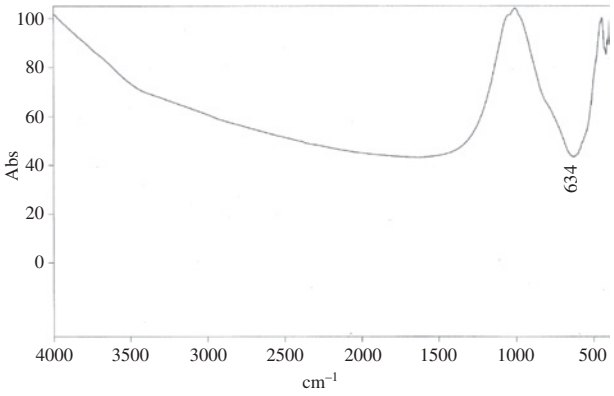

Figure 13: The FT-IR spectra of the TiO_2 nanoparticles.

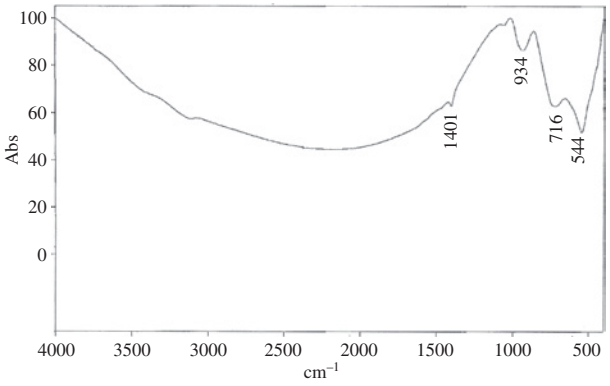

Figure 14: The FT-IR of the $PbFe_{12}O_{19}$-TiO_2 nanocomposites.

Scanning electron microscopy (SEM) was employed for the estimation of the morphology and the particle size of the products. The final particle size and morphology depend on the preparation conditions. Figure 4 shows the SEM images of the $PbFe_{12}O_{19}$ nanoparticles without any surfactant. The SEM images of the $PbFe_{12}O_{19}$ nanoparticles with capping salicylic acid are presented in Figure 5. As can be seen, the average particle size is approximately 60 nm. Figure 6 presents the SEM images of the $PbFe_{12}O_{19}$ nanoparticles with capping glucose as the surfactant. This image shows that nanoparticles are agglomerated. Figure 7 presents the SEM images of the $PbFe_{12}O_{19}$ nanoparticles with capping gelatine. The result confirms the obtained mono-disperse nanorods with an average size of around 70 nm. The SEM images of the $PbFe_{12}O_{19}$

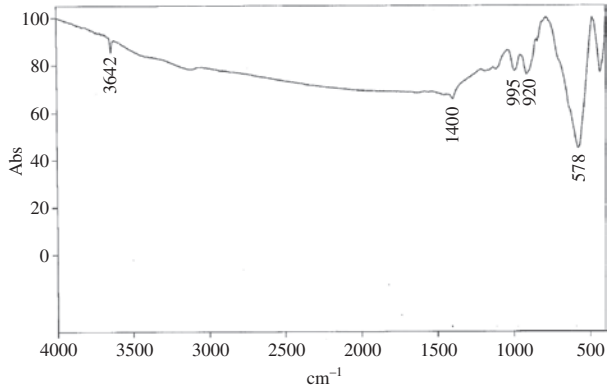

Figure 12: The FT-IR spectra of the $PbFe_{12}O_{19}$ nanoparticles.

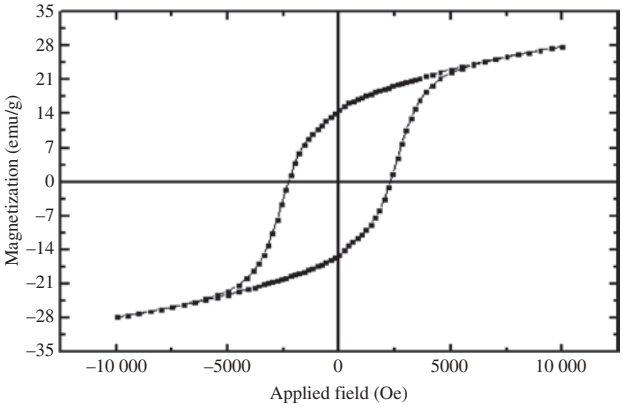

Figure 15: The VSM curves of the $PbFe_{12}O_{19}$ nanoparticles calcined at 800°C.

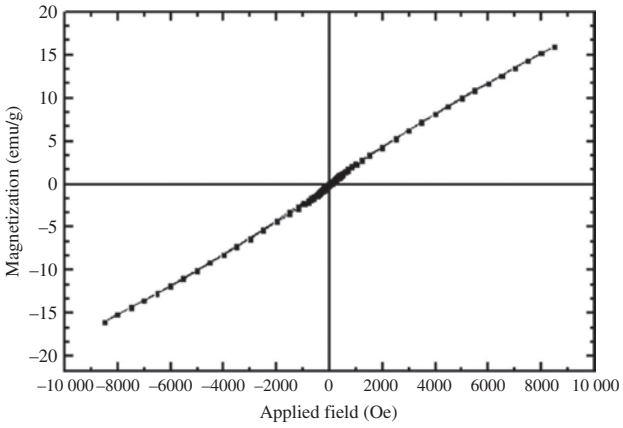

Figure 16: The VSM curves of the $PbFe_{12}O_{19}$-TiO_2 nanocomposites calcined at 500°C.

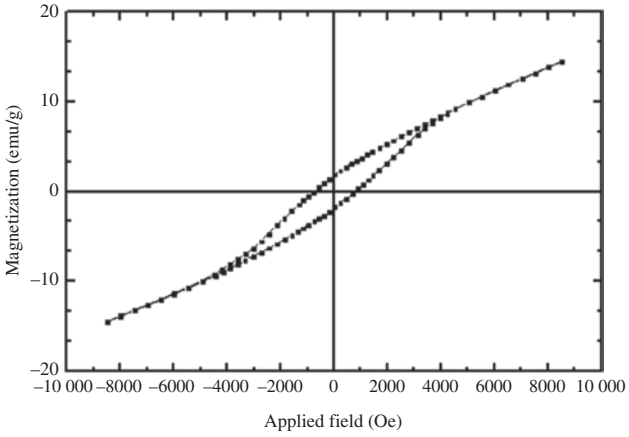

Figure 17: The VSM curves of the $PbFe_{12}O_{19}$-TiO_2 nanocomposites calcined at 800°C.

nanoparticles prepared by starch coating are shown in Figure 8. The images confirm the obtained mono-disperse nanoparticles with an average size of around 60 nm. Using starch as a natural surfactant leads to better nucleation. Figure 9 presents the SEM images of the TiO_2 nanoparticles prepared via the sol-gel method. The result confirms the obtained mono-disperse nanoparticles with an average size under 50 nm. Figure 10 illustrates the SEM images of the $PbFe_{12}O_{19}/TiO_2$ nanocomposite. The result confirms the obtained nanocomposite, which is agglomerated and has an average particle size of around 70 nm.

Figure 11 shows the transmission electron microscopy (TEM) images of the $PbFe_{12}O_{19}/TiO_2$ nanocomposite. As can be seen, the particle size is nearly 80 nm. Meanwhile, Figure 12 shows the Fourier transform infrared (FT-IR) spectra of the prepared $PbFe_{12}O_{19}$ nanoparticles. As can be seen, the absorption band at 578 cm^{-1} is assigned to the stretching mode of the Fe-O bond and the 920 and 995 cm^{-1} bands can be attributed to the stretching mode of the Pb-O bond. The spectra exhibit a broad absorption peak around 1400 cm^{-1}, the band corresponding to the stretching mode of C-C. The 642 cm^{-1} band is assigned to the O–H bending vibration mode due to the adsorption of moisture on the surface of the nanoparticles. Figure 13 shows the FT-IR spectra of the TiO_2 nanoparticles calcinated at 500°C. The absorption band at 643cm^{-1} is assigned to the stretching mode of the Ti-O bonds, which adsorbed on the surface of nanostructures. The FT-IR spectra of the $PbFe_{12}O_{19}$-TiO_2 nanocomposite is shown in Figure 14. The absorption bands at 544 and 716 cm^{-1} are assigned to the stretching modes of the Fe-O and Ti-O bonds. The spectra exhibit a broad absorption peak at around 934 cm^{-1} for the stretching mode of the Pb-O bond, and finally 1401 cm^{-1} is assigned to the stretching mode of the C-C bond.

The magnetic properties of the $PbFe_{12}O_{19}$ nanoparticles and $PbFe_{12}O_{19}$-TiO_2 nanocomposite were studied by using a vibrating sample magnetometer (VSM). Figure 15 shows the hysteresis loops for the $PbFe_{12}O_{19}$ nanoparticles. The results indicate that the sample exhibits ferromagnetic property and that a saturation magnetization of around 28 emu/g and coercivity of about 2100 Oe have been achieved. The magnetic property of the $PbFe_{12}O_{19}$-TiO_2 nanocomposite calcined at 500°C is shown in Figure 16. The result indicates that the saturation magnetization of

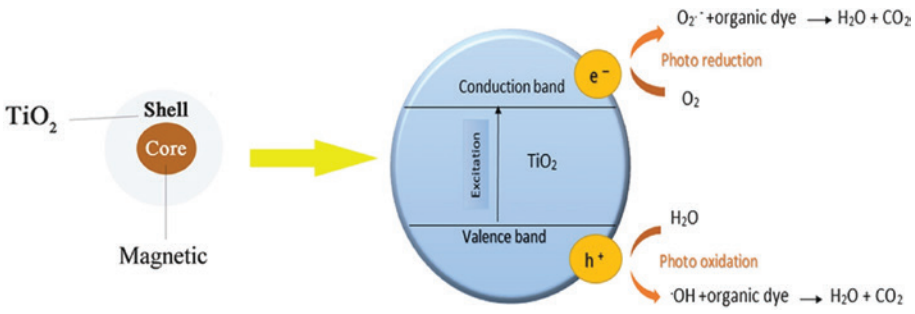

Figure 18: The photocatalyst mechanism in the degradation of toxic dyes.

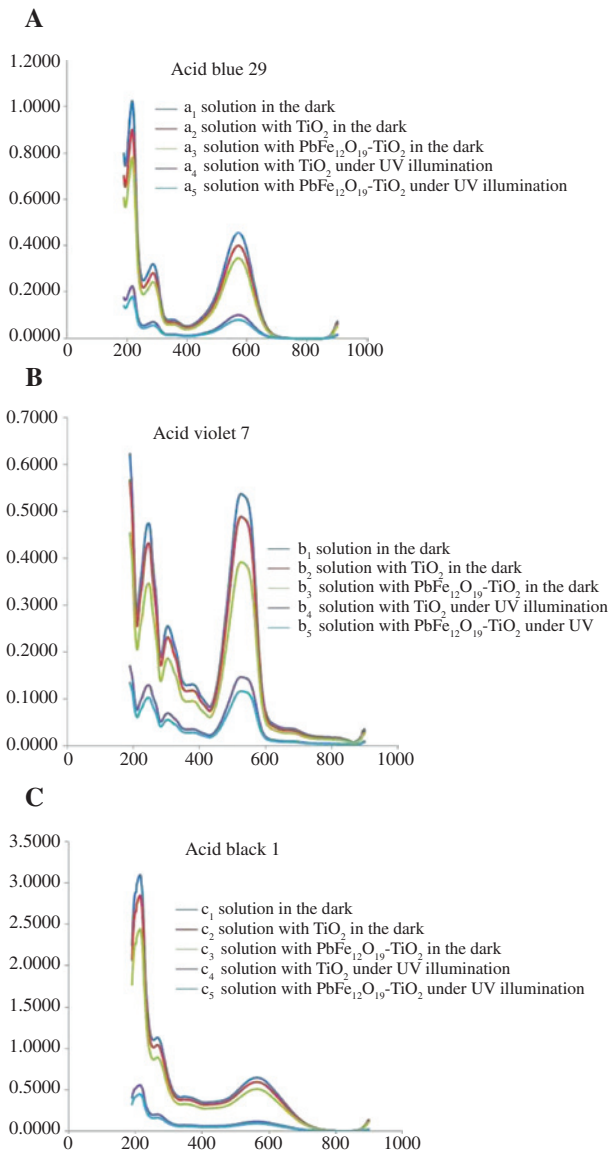

Figure 19: The UV-Vis absorption of the dyes in the presence of photocatalysts (A) acid blue 29, (B) acid violet 7 and (C) acid black 1.

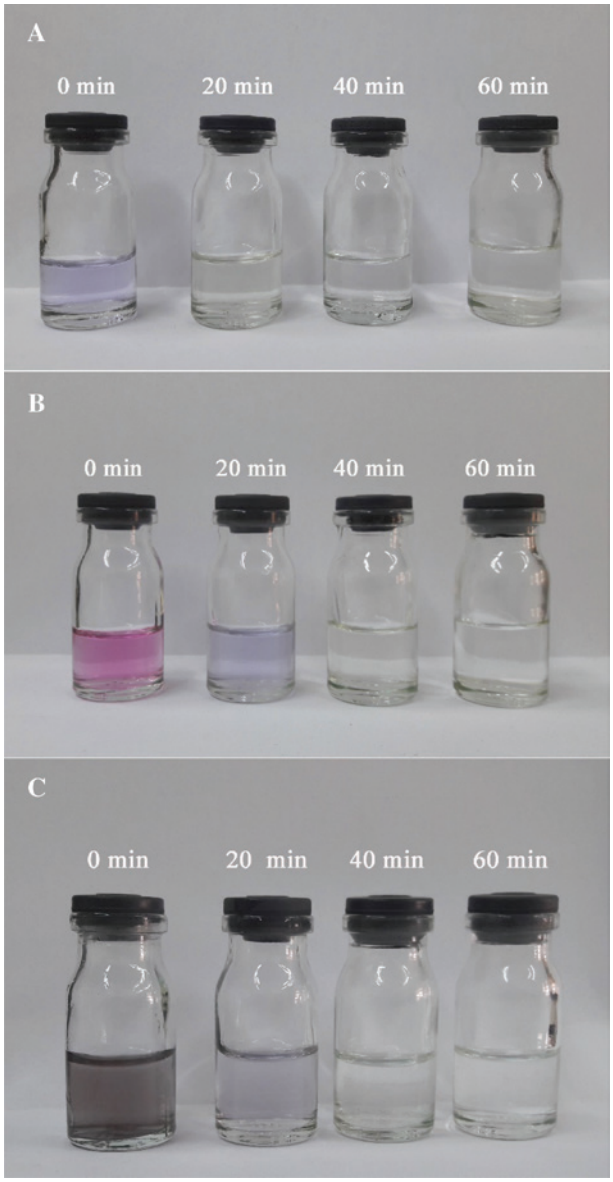

Figure 20: The photodegradation by the $PbFe_{12}O_{19}$/TiO_2nanocomposites of (A) acid blue 29, (B) acid violet 7 and (C) acid black 1.

around 16 emu/g and coercivity of about 0.4 Oe have been achieved. Figure 17 shows the magnetization curve of the $PbFe_{12}O_{19}$-TiO_2 nanocomposite calcined at 800°C. The results indicate that the sample exhibits ferromagnetic behaviour with coercivity of about 981 Oe and saturation magnetization of around 14 emu/g.

When the nanocomposite formed and calcined at 500°C, the amount of coercivity decreased. In comparison, when the calcination temperature increased to about 800°C, the amount of coercivity increased and the nanocomposite demonstrated ferromagnetic behavior. The results indicate that the amount of coercivity is increased by increasing the temperature of nanocomposite calcination from 500°C to 800°C.

The prepared nanocomposite has potential applications in improving environmental problems associated with toxic water pollutants. The mechanism of the photodegradation of toxic azo dyes under UV irradiation in the presence of the $PbFe_{12}O_{19}$-TiO_2 nanocomposite as an effective photocatalyst is shown in Figure 18. Azo dyes were exposed to UV light in the presence of this nanocomposite. The changes in the concentration of maximum wavelength dye are illustrated in Figure 19, which shows the UV absorptions of acid black 1, acid violet 7 and acid blue 29. The absorption curves of the solutions for all three acids do not show observable changes for these three conditions: dye solution in the dark, dye solution under illumination

and dye solution with the $PbFe_{12}O_{19}$ nanoparticles under illumination (19-a1, b1, c1). The degradation rates of the azo dyes in both UV illumination for the pure TiO_2 nanoparticles (19-a4, b4, c4) and the $PbFe_{12}O_{19}$-TiO_2 nanocomposites (19-a5, b5, c5) are more effective than those under the following conditions: pure TiO_2 nanoparticles in the dark (19-a2, b2, c2) and $PbFe_{12}O_{19}$-TiO_2 under illumination (19-a3, b3, c3). This is due to the formation of extra produced electron-hole levels as new traps in the TiO_2 nanoparticles by composition with the $PbFe_{12}O_{19}$ levels. The UV absorption rates of the decomposition of the azo dyes for exposure times of 20, 40 and 60 to the nanocomposite are shown in Figure 20. With increasing UV irradiation time, the dye concentration decreased rapidly and toxic dyes decomposed to carbon dioxide, water and other less or non-toxic residuals.

Conclusions

In conclusion, the synthesis, characterization and photocatalytic activity of the $PbFe_{12}O_{19}$-TiO_2 nanocomposites were reported. By investigating the effects of different surfactants on the lead hexa ferrites in the SEM images, we found that starch – as a natural surfactant – causes the growth and formation of mono-disperse nanoparticles and induces uniformity than other surfactants. The TEM image of the nanocomposite obtained and the grain size are under 100 nm. This confirms the crystallite size obtained the from Debye-Scherer equation. VSM results confirmed that, if temperature calcination is increased to around 800°C, the ferromagnetic behaviour becomes highly apparent. The photocatalytic behavior of thte $PbFe_{12}O_{19}$-TiO_2 nanocomposite was investigated for the composition of various azo dyes under UV irradiation. The results showed that the sol-gel method is a suitable method for the preparation of the $PbFe_{12}O_{19}$-TiO_2 nanocomposite, which is an ideal material for use in photocatalytic applications to remove toxic dyes.

Experimental

Materials and methods

The materials used in the study, namely, $Pb(NO_3)_2$ $4H_2O$, $Fe(NO_3)_3$ $9H_2O$, NaOH, salicylic acid, glucose, starch, gelatine, tetra isopropyl ortho titanate (TTIP), nitric acid and methanol, were all purchased from Merck or Aldrich (Berlin, Germany). All the chemicals were used as received without further purification. A multi-wave ultrasonic generator (Band line MS 73), with a converter/transducer and titanium oscillator, operating at 20 kHz with a maximum power output of 150 W, was used for the ultrasonic irradiation. Room temperature magnetic properties were investigated using the VSM device (Meghnatis Kavir Kashan Company, Iran) in an applied magnetic field sweeping between ± 10 000 Oe. The XRD patterns were recorded by a Philips X-ray diffractometer using Ni-filtered CuKα radiation (Amsterdam, Netherlands). The SEM images were obtained using a LEO instrument model 1455VP (Cambridge, UK). Prior to taking the images, the samples were coated by a very thin layer of Pt (using a BAL-TEC SCD 005 sputter coater, CA, USA) to make the sample surface a conductor and to obtain better contrast.

Synthesis of the $PbFe_{12}O_{19}$ nanoparticles

First, 1.46 g of $Fe(NO_3)_3$ $9H_2O$ were dissolved in 200 mL of deionized water, to which 0.2 g of $Pb(NO_3)_2$ $4H_2O$ was added after 10 min. After the dissolution of materials, 10 mL of NaOH (1M) was slowly added to the solution until a pH of 10 was achieved. A brown precipitate was then centrifuged and rinsed with distilled water. Next, the obtained precipitate was dried at 80°C and finally calcined at 800°C, thus revealing the magnetic feature of the sample. Subsequently, various organic surfactants were used to synthesize the lead ferrite and investigate its effect on the crystalline morphology.

Synthesis of the TiO_2 nanoparticles

The TiO_2 nanoparticles were prepared by the sol-gel method with 1.25 g of tetra isopropyl ortho titanate (TTIP), as the raw material, mixed with 25 mL of methanol in a dry atmosphere and held for 10 min. After that, 5 mL of distilled water was added. In this level, the white sol was formed. Sol was stirred for 20 min, after which 2 mL of HNO_3 was slowly added until a pH level of 2 was achieved. A yellowish transparent gel was formed after 90 min stirring. In the final step, the obtained powder was calcined at 500°C for 2 h.

Synthesis of the $PbFe_{12}O_{19}$-TiO_2 nanocomposite

About 0.21 g of $PbFe_{12}O_{19}$ (capping starch) was dispersed in 25 mL of methanol and 1.25 g TTIP. After 10 min, the solution was stirred and 5 mL of distilled water was added to the mixture. After 20 min, we slowly added 2 mL of HNO_3 until reaching a pH level of 2. In this level, the solution was stirred for 90 min until the white gel was formed. The obtained gel was dried at 80°C for 2 h. In the next step, the obtained powder was calcined at 500°C for 2 h. In the final step, because the powder did not find a magnetic state for the first time, it was calcined again to 800°C for 5 h.

Photocatalytic degradation process

The removal of the azo dyes from a solution under UV light was performed in the presence of the $PbFe_{12}O_{19}$-TiO_2 nanocomposite as a photocatalyst sample. In each photocatalysis test, 0.1 g catalyst and 5 mL of the dye solution (10 ppm) were stirred with a magnetic stirrer in darkness under UV-visible light to determine the adsorption of the dye by the catalyst. The solution was irradiated by a 10 W UV lamp

that was placed in a quartz pipe in the middle of the reactor. The solution was centrifuged every 20 min and the level of photodegradation was recorded.

References

Augugliaro, V.; Loddo, V.; Pagliaro, M.; Palmisano, G.; Palmisano, L. Clean by light irradiation: practical applications of supported TiO_2. Royal Society of Chemistry: London, UK, 2010.

Chaudhury, S.; Rakshit, S. K.; Parida, S. C.; Singh, Z.; Mudher, K. S.; Venugopal, V. Studies on structural and thermo-chemical behavior of $MFe_{12}O_{19}$ (s)(M=Sr, Ba and Pb) prepared by citrate–nitrate gel combustion method. *J. Alloys Compd*. **2008**, *455*, 25–30.

Cosnier, S.; Gondran, C., Senillou, A.; Grätzel, M.; Vlachopoulos, N. Mesoporous TiO_2 films: new catalytic electrode fabricating amperometric biosensors based on oxidases. *Electroanalysis* **1997**, *9*, 1387–1392.

Ebrahimi, Z.; Hedayati, K.; Ghanbari, D. Preparation of hard magnetic $BaFe_{12}O_{19}$–TiO_2nanocomposites: applicable for photo-degradation of toxic pollutants. *J. Mater. Sci. Mater. Electron*. **2017**, *28*, 13956–13969.

Fujishima, A.; Honda, K. Electrochemical photolysis of water at a semiconductor electrode. *Nature* **1972**, *238*, 37–38.

Ghanbari, D.; Sharifi, S.; Naraghi, A.; Nabiyouni, G. Photo-degradation of azo-dyes by applicable magnetic zeolite Y–Silver–$CoFe_2O_4$ nanocomposites. *J. Mater. Sci. Mater. Electron*. **2016**, *27*, 5315–5323.

Gawande, M. B.; Luque, R.; Zboril, R. The rise of magnetically recyclable nanocatalysts. *Chem Cat Chem*. **2014**, *6*, 3312–3313.

Hamnett, A.; Dare-Edwards, M. P.; Wright, R. D.; Seddon, K. R.; Goodenough, J. B. Photosensitization of titanium (IV) oxide with tris (2, 2′-bipyridine) ruthenium (II) chloride. Surface states of titanium (IV) oxide. *J. Phys. Chem*. **1979**, *83*, 3280–3290.

Hedayati, K.; Goodarzi, M.; Kord, M. Green and facile synthesis of Fe_3O_4-PbS magnetic nanocomposites applicable for the degradation of toxic organic dyes. *Main Group Metal Chem*. **2016**, *39*, 183–194.

Hoffmann, M. R.; Martin, S. T.; Choi, W.; Bahnemann, D. W. Environmental applications of semiconductor photocatalysis. *Chem. Rev*. **1995**, *95*, 69–96.

Jafari, M.; Sobhani, A.; Salavati-Niasari, M. Effect of preparation conditions on synthesis of Ag_2Se nanoparticles by simple sonochemical method assisted by thiourea. *J. Ind. Eng. Chem*. **2014**, *20*, 3775–3779.

Li, Y.; Lee, N. H.; Lee, E. G.; Song, J. S.; Kim, S. J. The characterization and photocatalytic properties of mesoporousrutile TiO_2 powder synthesized through self-assembly of nano crystals. *Chem. Phys. Lett*. **2004**, *389*, 124–128.

Linsebigler, A. L.; Lu, G.; Yates Jr, J. T. Photocatalysis on TiO_2 surfaces: principles, mechanisms, and selected results. *Chem. Rev*. **1995**, *95*, 735–758.

Liu, B.; Wang, Z.; He, J. SiO_2/TiO_2 multilayer films grown on cotton fibers surface at low temperature by a novel two-step process. *Mater. Lett*. **2012**, *67*, 8–10.

Liu, Q.; Liu, H.; Han, M.; Zhu, J.; Liang, Y.; Xu, Z.; Song, Y. Nanometer-sized nickel hollow spheres. *Adv. Mater*. **2005**, *17*, 1995–1999.

Masoumi, S.; Nabiyouni, G.; Ghanbari, D. Photo-degradation of azo dyes: photo catalyst and magnetic investigation of $CuFe_2O_4$–TiO_2 nanoparticles and nanocomposites. *J. Mater. Sci. Mater. Electron*. **2016**, *27*, 9962–9975.

Matthews, R. W. Purification of water with near—UV illuminated suspensions of titanium dioxide. *Water Res*. **1990**, *24*, 653–660.

Moumen, N.; Pileni, M. P. New syntheses of cobalt ferrite particles in the range 2–5 nm: comparison of the magnetic properties of the nanosized particles in dispersed fluid or in powder form. *Chem. Mater*. **1996**, *8*, 1128–1134.

Mutzhas, M. F.; Hölzle, E.; Hofmann, C.; Plewig, G. A new apparatus with high radiation energy between 320–460 nm: physical description and dermatological applications. *J. Invest. Dermatol*. **1981**, *76*, 42–47.

Peral, J.; Domenech, X.; Ollis, D. F. Heterogeneous photocatalysis for purification, decontamination and deodorization of air. *J. Chem. Technol. Biotechnol*. **1997**, *70*, 117–140.

Song, Q.; Zhang, Z. J. Shape control and associated magnetic properties of spinel cobalt ferrite nanocrystals. *J. Am. Chem. Soc*. **2004**, *126*, 6164–6168.

Sutin, N.; Creutz, C. Properties and reactivities of the luminescent excited states of polypyridine complexes of ruthenium (II) and osmium (II). **1977**, *168*, 1–27.

Thompson, G. K.; Evans, B. J. The structure–property relationships in M-type hexaferrites: hyperfine interactions and bulk magnetic properties. *J. Appl. Phys*. **1993**, *73*, 6295–6297.

Xiao, S. H.; Jiang, W. F.; Li, L. Y.; Li, X. J. Low-temperature autocombustion synthesis and magnetic properties of cobalt ferrite nanopowder. *Mater. Chem. Phys*. **2007**, *106*, 82–87.

Xin, T.; Ma, M.; Zhang, H.; Gu, J.; Wang, S.; Liu, M.; Zhang, Q. A facile approach for the synthesis of magnetic separable Fe_3O_4@TiO_2, core–shell nanocomposites as highly recyclable photocatalysts. *Appl. Surf. Sci*. **2014**, *288*, 51–59.

Yang, N.; Yang, H.; Jia, J.; Pang, X. Formation and magnetic properties of nanosized $PbFe_{12}O_{19}$ particles synthesized by citrate precursor technique. *J. Alloys Compd*. **2007**, *438*, 263–267.

Zhang, Q.; Gao, L.; Guo, J. Effects of calcination on the photocatalytic properties of nanosized TiO_2 powders prepared by $TiCl_4$ hydrolysis. *Appl. Catal. B Environ*. **2000**, *26*, 207–215.